Reapplication Potential of Historic Pb-Zn Slag in Regard to Net Zero Principles

Dragan Radulović , Anja Terzić * , Jovica Stojanović , Vladimir Jovanović , Dejan Čedomir Todorović , Branislav Božidar Ivošević

Posted Date: 28 November 2023

doi: 10.20944/preprints202311.1730.v1

Keywords: critical raw materials; alternative deposits; secondary resources; building materials; instrumental analyses; microscopy.

Article

Reapplication Potential of Historic Pb-Zn Slag in Regard to Net Zero Principles

Dragan Radulović [1], Anja Terzić [2,*], Jovica Stojanović [1], Vladimir Jovanović [1], Dejan Todorović [1] and Branislav Ivošević [1]

[1] Institute for Technology of Nuclear and Other Mineral Raw Materials, Franchet d'Esperey 86, 11000 Belgrade, Serbia
[2] Institute for Materials Testing - IMS, Bulevar Vojvode Mišića 43, 11000 Belgrade, Serbia
* Correspondence: anja.terzic@institutims.rs

Abstract: Smelting used to be less efficient in the past, so wastes obtained from historical processing at smelter plants usually contain certain quantities of valuable metals. A case study was conducted, which included an investigation of the physicochemical, mineralogical, and microstructural properties of raw material found at the historic slag pond near the Topilnica Veles smelter in North Macedonia. The Pb-Zn slag was sampled using traditional geophysical methods such as drill holes and pitholes. The mineralogical and microstructural analysis revealed that the Pb-Zn slag is a very complex and inhomogeneous alternative raw material with utilizable levels of metals, specifically Pb (2.24 wt%), Zn (7.10 wt%), and Ag (27.53 ppm). Amorphous phase, lead alloys, zinc alloys, wurtzite, sphalerite, galena, cerussite, elemental silver, elemental copper, elemental iron, magnetite, spinel, rutile, hematite, and troilite were also identified through qualitative mineralogical analysis. The glassy matrix composed of spinel, silicates, and mixed spinel-silicate is the most abundant constituent in slag composition. The various potential applications of the slag are possible based on its mineralogical and geochemical properties. Because the extraction of Pb, Zn, and Ag has certain economic potential, the next step, which will include gravity concentration and magnetic separation procedures, will be to form metal concentrates into their collective concentrate, from which the maximum amount of silver can be extracted. Slag's amorphous spinel, silicate, and mixed spinel-silicate phases, which contain high concentrations of SiO_2, Al_2O_3, CaO, and Fe_2O_3, are suitable for use in building materials such as cement clinker, filler, or aggregate for concrete or mortar. The goal of this research is to close the circle of slag's reutilization potential in terms of Net Zero and Zero Waste principles, so it is critical to thoroughly investigate the material and establish methods and preparation processes, as well as ways of concentrating useful components into commercial products.

Keywords: critical raw materials; alternative deposits; secondary resources; building materials; instrumental analyses; microscopy

1. Introduction

After copper and aluminum, zinc and lead are the two non-ferrous metals that are utilized most frequently in various industrial branches [1]. In 2022, the amount of zinc mined worldwide was 13 million tons [2,3]. According to the GHG Protocol Standard's methodology, the carbon footprint of zinc production is approximately 0.93 tons CO_2e per ton of zinc [4]. Zinc is mostly used in the galvanizing process, which keeps steel and iron from rusting. In addition, zinc can be alloyed with other metals to create die-cast items like door handles, brass by alloying it with copper, and bronze by alloying it with tin and copper. In 2022, a total of 4.49 million metric tons of lead were mined worldwide [2]. Lead has several applications, including as a radiation shield, fusible alloys, lead-acid batteries, and building construction [5]. Lead has a much smaller carbon footprint than zinc, ranging from 30 to 76 kg CO_2/kg of material, according to the EPA [6].].

Heavy metals with high concentrations, such as lead and zinc, are usually found in waste materials produced during the metal mining and smelting processes [7]. Although hydrometallurgical processes now account for the majority of the world's production of both of these metals due to environmental concerns, pyrometallurgical processing still contributes 10% to 20% of

Zn and Pb production [8]. Smelter slags are a source of 70 and 7 kt/y of Zn and Pb, respectively [1]. Zinc and lead are found both mainly in amorphous phases but also as ZnO, ZnS, Pb apatite, and $PbSO_4$ [1].

Due to a lack of economically viable technology, the vast majority of these waste materials are disposed of or temporarily stored in non-hazardous industrial solids storage facilities or in open landfills. The problem is that slag from metallurgical processes is a significant source of pollutants such as the previously mentioned heavy metals and sulfide minerals, which are extremely hazardous to human health as well as the aquatic and soil environments, even when standard control measures have been implemented [9–11]. Current methods of treating metallurgical slags, such as reprocessing, desulfurization, backfilling, and restoration, are not widely used due to their high cost and/or low efficiency [12]. Waste materials placed near closed mining sites or smelters in isolated rural areas, in particular, have received much less attention because the local government cannot afford the high costs associated with managing and disposing of them in an environmentally responsible manner. Therefore, it is essential to develop waste treatment solutions that are economically, environmentally, and technically feasible [13,14].

Due to its suitable mineralogical and geochemical properties, various potential applications of the Pb-Zn slag are possible. Namely, the extraction of valuable metals such as Pb, Zn, and Ag has economic potential. Therefore, methods such as gravity concentration and magnetic separation are employed to create metal concentrates into their collective concentrate, from which the maximum amount of one or several elements can be extracted [15,16]. Production of construction material could be a viable way to sustainably utilize Pb and Zn slags with a financial return, given their quantity and mineralogical composition, especially if the final products could be manufactured and sold locally [17]. This coincides with the 17 sustainable development goals (SDGs) proposed by the United Nations to advance social and environmental justice under the 2030 Agenda for Sustainable Development [18,19]. The 2030 Agenda emphasizes the need for sustainable management of the environment and its resources, and the mining sectors, including metallurgy, are under pressure to create sustainable technologies in order to meet the relevant SDGs.

The application of a recycled material in the construction industry can be demanding if all sides of the problem are to be taken into account: proper application for the secondary raw material, economic viability of the final product, and its environmental impact. Various methods for reapplication of Pb-Zn metallurgical slag have been proposed so far. To estimate the potential use of lead-zinc slag as a construction material, the properties in fresh and hardened states as well as the durability of various mixes of mortar, concrete, geopolymer, alkali-activated material (AAM), and brick were assessed. The majority of the studies demonstrated these mixes' good performance as building materials. For example, from the standpoint of mechanical properties, lead-zinc slag could replace up to 50% of the raw materials in mortar and concrete mixes. Lead-zinc slag can increase the physico-mechanical and durability characteristics of concrete and mortar mixtures, even at higher replacement rates. [20–23]. It can also increase the durability properties of self-compacting concrete (SCC) mixes by up to 25%. One important problem brought on by the disposal of lead-zinc slag is leaching, which can be effectively controlled by preparing mortar, concrete, geopolymer, and AAM [20]. Industrial byproducts like metallurgical slags, ashes, and mine tailings have been used as raw materials to make sintered, autoclaved, and unfired (adobe) bricks [24]. For example, hematite mine tailing mixed with pozzolanic materials was used to make traditional fired and autoclaved bricks. However, producing both types of bricks requires a lot of energy, high temperatures, and the emission of air pollutants and greenhouse gases [25,26]. To cut down on energy use and carbon emissions, more and more people are interested in producing environmentally friendly and sustainable unfired bricks to replace fired building products [27]. Also, the preparation of high-value glass-ceramic using lead slag and lead-zinc tailings can reduce pollution from slag landfills in order to accomplish comprehensive waste utilization [28]. In keeping with the growing trend towards waste reutilization and clean production, geopolymers were synthesized to immobilize Pb^{2+} and Zn^{2+} by simultaneously using electrolytic manganese residue and lead-zinc smelting slag as raw aluminosilicate materials. In this case, the effects of Ca, Al, and Si on the compressive strengths of

 doi:10.20944/preprints202311.1730.v1

geopolymers were examined by utilizing different amounts of supplementary cementitious materials, namely silica-gel powder, sodium aluminate, and blast furnace slag. Furthermore, the geopolymers can be used to immobilize two heavy metals, Pb and Zn [29]. There are various applications for Pb-Zn slags in construction practice. If the slags are similar to sand in terms of their granularity and particle size, they may be utilized as fine aggregate in concrete [30]. Thereby, Pb-Zn slags can also be used as a pozzolanic admixture, as structural fill material in road construction and embankments, or as a base material for making bricks and tiles after undergoing the required processing, such as grinding [31–34]. Arsenic from wastewater from copper smelting has recently been successfully removed using zinc slag, allowing for the wastewater's safe discharge [35]. Due to their excellent mechanical performance, alkali-activated materials have gained popularity recently. They are made by combining alkali solutions with solid precursors such as metakaolin, slag, and fly ash. When AAMs made with Pb-Zn slag were tested, it was discovered that the leaching of heavy metals from the slag had decreased and was below allowable limits [36,37].

One issue that has not been thoroughly examined up to this point is the reapplication of Pb-Zn slag as coarse aggregate or a component of it in the design of concrete or mortar. The building industry requires a lot of natural resources to produce high-quality concrete due to increasing global urbanization. Natural aggregates, both fine and coarse, usually make up three-fourths of the concrete volume. Therefore, the search for alternative materials originating usually from industrial processes as well as construction and demolition waste as a substitute for aggregates in concrete production is a good solution for this problem. The goal is to lower the cost of concrete manufacturing, the amount of energy used, and the amount of CO_2 emitted. As a result of the application of waste materials, landfill space is eliminated and repurposed, and the problem of natural resource depletion is alleviated. Reusing PB-Zn slag before or after the extraction of valuable metals such as Pb, Zn, and Ag makes it possible to achieve a number of Sustainable Development Goals (SDGs), including promoting life on land (SDG 15), ensuring that everyone has access to clean water and sanitation (SDG 6), industry, innovation, and infrastructure (Goal 9), responsible consumption and production (SDG 12), and combating climate change (SDG 13). In this regard, using Pb-Zn slag from smelter plants may represent one of the most promising possibilities for waste consumption and reapplication in civil engineering. Therefore, the detailed characterization of historic Pb-Zn slag from the smelter Topilnica Veles is conducted in order to assess both the possibility of extracting the valuable metals and reusing the slag as alternative raw material in building industry.

2. Materials and Methods

The technogenic mineral raw material (Pb-Zn slag) from the smelter Topilnica Veles, North Macedonia (KEPS MONT GROUP Skopje) was investigated. There are currently 2,000,000 t of historic Pb-Zn slag located at the landfill near the smelter (Figures 1 and 2).

Figure 1. Proximity of the nearest urban settlement from the smelter and landfill (source Google Maps).

Preprints (www.preprints.org) | NOT PEER-REVIEWED | Posted: 28 November 2023 doi:10.20944/preprints202311.1730.v1

Figure 2. Disposition of the open-air landfill near smelter plant (source Google Maps).

The Pb-Zn slag was physicochemically and mineralogically characterized in order to assess the possibility of the valorization of useful metals and subsequently the slag's reapplication in the civil engineering industry. Figure 3 depicts the scheme of the employed experimental design. Once the applied methods and instrumental techniques have determined the relevant characteristics of the analyzed alternative mineral raw material, it will be possible to define all of the required parameters as a basis for further technological tests. This will eventually lead to the best procedure for valorizing Pb-Zn slag from Topilnica Veles, allowing for the development of innovative technological solutions and commercial building products.

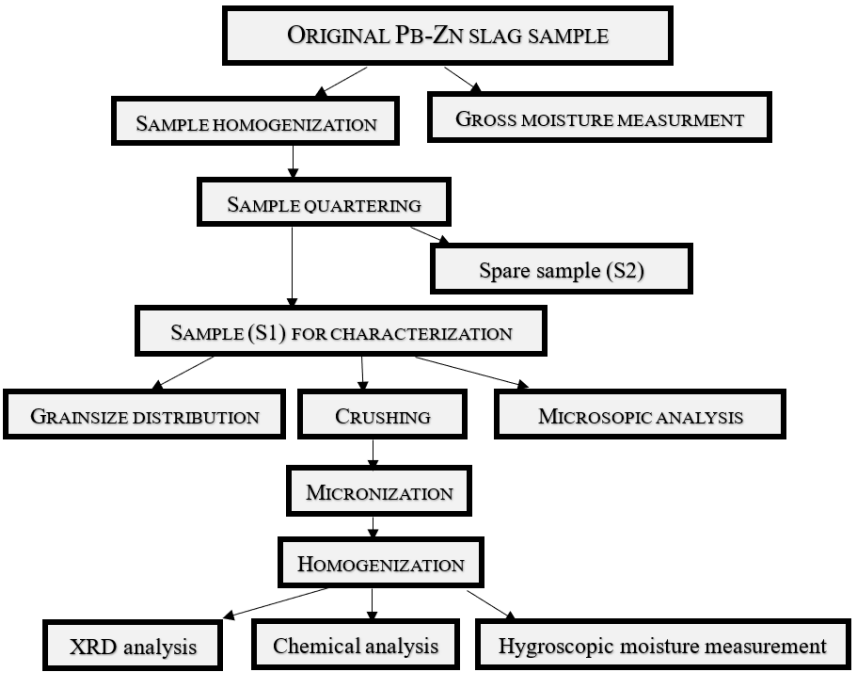

Figure 3. Scheme of the experimental design for characterization of Pb-Zn slag.

2.1. Sampling and laboratory processing of Pb-Zn slag specimens

The entire characterization was conducted on a representative sample of 50 kg of Pb-Zn slag obtained directly from the historic landfill located near the smelter plant (Figure 2). The mean grain

 doi:10.20944/preprints202311.1730.v1

diameter of the representative sample was 5.0 + 0.00 mm. The procedure was conducted as described in Figure 3.

A share of the raw material was taken from the initial Pb-Zn slag sample in order to calculate the gross moisture content. The primary (original) slag sample was then homogenized. Following homogenization, the obtained raw material was split into two samples (S1 and S2) using the quartering method. The S2 sample was reserved, and the other half, i.e., the S1 sample, was used for further characterization as follows: (1) Employing Tyler's standard series of sieves, the grain-size distribution was determined using 5 kg of the original sample. (2) The second part of this sample was used in a microscopic analysis to assess the presence and potential quantity of useful minerals contained in the slag. (3) The third part of the sample underwent crushing (jaw and roll crushers) and micronization (vibratory disc mill) to the mean particle size adequate for X-ray diffraction analysis, chemical analysis, and further physico-chemical characterization.

2.2. Physical characterization of the Pb-Zn slag sample (moisture content)

The original Pb-Zn slag sample was removed from the sacks in which it was distributed to the laboratory and measured for gross moisture as the first step in the physical characterization of this secondary raw material.

The Pb-Zn slag sample's gross moisture was determined using the standard method. Namely, the gross moisture content was calculated on three initial samples of Pb-Zn slag from Topilnica Veles with an average grain size of -5.0+0.00 mm. The samples were initially dried at room temperature (20±2°C) for 24 hours. The gross moisture content (M_g) was calculated using the following equation (Eq. 1):

$$M_g = \frac{(m_{os} - m_{ads})}{m_{os}}, (\%) \quad (1)$$

where m_{os} is the mass of the original slag sample (g) and m_{ads} is the mass of the slag sample dried at ambient temperature (g).

The calculated value is the arithmetic mean of the measured values for each of the three samples. The initial samples of Pb-Zn slag had a gross moisture content of 0.0957%, according to the measurements.

The Pb-Zn slag sample was homogenized afterwards, and its granulometric composition was determined by sieving through a standard Tyler series of sieves. The hygroscopic moisture of Pb-Zn slag samples was determined after crushing them to an average grain size of 0.2 mm. Hygroscopic moisture was also calculated on a total of three samples. Prior to hygroscopic moisture determination, the samples were dried at 105°C for 4 hours. The hygroscopic moisture content (M_h) of the samples was calculated as the mean of three measurements using the equation (Eq. 2):

$$M_h = \frac{(m_s - m_{ds})}{m_s}, (\%) \quad (2)$$

where m_s is the mass of the slag sample upon crushing (g), and m_{ds} is the mass of the slag sample dried at 105°C (g).

The obtained result for the hygroscopic moisture content of the investigated Pb-Zn slag was 0.11%.

Both gross and hygroscopic moisture content values are within acceptable limits for use in concrete, as most fine aggregates have a maximum drained moisture content of about 3% to 8%, whereas coarse aggregates have a maximum drained moisture content of about 1% to 6%.

2.3. Grainsize distribution analysis of Pb-Zn slag

The grain size distribution was analyzed on the starting sample of Pb-Zn slag (mean grain size: 5 mm), as it was already mentioned. The initial sample of Pb-Zn slag's granulometric composition was determined by sieving on Tyler's series of sieves[1], with the last sieve in the opening sequence being 0.1 mm.

[1] https://wstyler.com/particle-analysis/test-sieves/wstyler-test-sieves/

 doi:10.20944/preprints202311.1730.v1

2.4. Instrumental analysis of Pb-Zn slag

Pb-Zn slag samples were dried at 105°C prior to pulverization in a vibratory disk mill (Herzog, Germany)[2] equipped with an HP-M 500 disc grinding mill designed to crush large amounts of material (100 g of material per sample was used in this experiment). The mill has grinding vessels made of chrome steel measuring 500 and 1000 cm^3. For X-ray fluorescence spectroscopy, the sample material is finely ground (the maximum grain size per sample was less than 2 mm). The mill operates in a semi-automated mode. For chemical analysis, energy-dispersive X-ray fluorescence (EDXRF) was employed. The X-ray tube in the EDXRF apparatus (Spectro Xepos, SPECTRO Analytical Instruments) has a current of 0.1 mA and is powered by a 50 kV generator. The Si-Drift Detector has a very high resolution of 170 eV with Peltier cooling and a 75 µm Be side window. In the experiment, Spectro X-Lab Pro, Version 2.2.2, was used as the software. A Specac press was used to prepare 5 g of sample material and 1 g of Cereox wax binder (Fluxana GmbH, Bedburg-Hau, Germany) at 20 t for 3 minutes. Quantities of Pb, Zn, S, and Ag were determined using the atomic absorption spectroscopy (AAS) technique on a PinAAcle 900 Perkin Elmer instrument. Pulverized slag samples (d50<63 µm) were used in the analysis.

A number of samples were subjected to mineralogical analysis. The first sample, which was the original Pb-Zn slag sample, was examined to see if any valuable minerals were present. Subsequently, the Pb-Zn slag sample was crushed to a size class of -2.38+0.00 mm. A sample was then taken from this and, following micronization, utilized for X-ray diffraction (XRD) analysis, which allowed for the determination of the sample's mineral composition. X-ray diffraction analysis was employed to determine and record the Pb-Zn sample's mineral phase composition. A Philips X-ray diffractometer, model PW-1710, equipped with a scintillation counter and a curved graphite monochromator, was used to analyze the sample. The intensities of the diffracted CuKα X-ray radiation (λ=1.54178Å) were measured at room temperature in intervals of 0.02 °2θ and 1 s in the range from 4 to 65 °2θ. The X-ray tube was loaded with a voltage of 40 kV and a current of 30 mA, while the slits for directing the primary and diffracted beams were 1° and 0.1 mm.

Preparations of slag samples for optical microscopic inspection are conducted in Plexiglas using medium-density grains. The preparation area was 2.2 cm^2. Carl Zeiss-Jena's JENAPOL-U polarizing microscope for transmitted and reflected light was used for the analysis, along with a measuring tool. Axiocam 105 color camera and software package Carl Zeiss AxioVision SE64 Rel. 4.9.1 with the Multiphase module was employed during the recording of the samples.

Scanning electron microscopy (SEM) was conducted on the micronized Pb-Zn samples that were used in optical microscopy analysis. The testing sample was coated with carbon (20 nm layer, density 2.25 g/cm^3). The textural analysis was conducted on a SEM instrument, the JEOL JSM-6610LV. The magnification of the device is 5 to 300,000 times. The instrument is equipped with an electron gun. The electron source is W wire, LaB 6. The voltage is 0.3–30 kV. The instrument works with a vacuum system: a rotary pump and turbomolecular pump (included in the basic configuration of the microscope), an ion pump (used for LaB6), and a rotary pump for working in low vacuum (10–270 Pa). Detectors are: SE detector; BSE detector; CL detector; and EDS detector (model: X-Max Large Area Analytical Silicon Drift connected with INCAEnergy 350 Microanalysis System). The detection of elements $Z \geq 5$; detection limit ~ 0.1 wt.%, resolution 126 eV Characteristics of the sample chamber: sample movement: 5-axis (X, Y, Z, T-tilt, R-rotation). Maximum sample size: 20 cm (width), 8 cm (height), 1 kg (weight). Two infrared cameras are included. Standards used for microanalysis: 64 natural minerals and synthetic compounds The device for evaporation of samples with gold (Au) and carbon (C) is model LEICA SCD005. Accompanying equipment: ultrasonic bath, binoculars, etc. A voltage of 20 kV and an extinction time of 50 s were used. The lower limit of EDX sensitivity is ~ 0.3%.

[2] https://www.herzog-maschinenfabrik.de/fileadmin/content/downloads/en/productbrochure/Herzog_HP-M_500_en_web.pdf

Preprints (www.preprints.org) | NOT PEER-REVIEWED | Posted: 28 November 2023 doi:10.20944/preprints202311.1730.v1

3. Results

This Following a sieve analysis of Tyler's set of sieves (Chapter 2.3), all of the first sieve's weights (M) as well as the last sieve's weights were measured. The acquired data are then arranged and presented in the form of Table 1. For the initial sample of Pb-Zn slag size -5 + 0.00 mm, a diagram of the granulometric composition with three curves, as shown in Figure 4, was created using the data from Table 1.

Table 1. Grain-size distribution of the original Pb-Zn slag sample from Topilnica Veles.

Size class (mm)	M (%)	↓∑ M (%)	↑∑ M (%)
+ 5.00	0.68	0.68	100.00
-5.00 + 3.35	0.35	1.03	99.32
-3.35 + 2.00	3.36	4.39	98.97
-2.00 + 1.25	8.21	12.60	95.61
-1.25 + 0.71	38.18	50.78	87.40
-0.71 + 0.50	21.20	71.98	49.22
-0.50 + 0.40	8.92	80.90	28.02
-0.40 + 0.30	10.31	91.21	19.10
-0.30 + 0.20	5.58	96.79	8.79
-0.20 + 0.10	2.59	99.38	3.21
-0.10 + 0.00	0.62	100.00	0.62
Input	100.00		

The average grain diameter (d_{50}) and particle size at which 80% of the material will pass when screened (d_{80}) of the Pb-Zn slag sample are 0.695 mm and 1.772 mm, respectively, as shown in Figure 4. The obtained grain-size distribution with certain modifications (addition of either natural or recycled concrete aggregate) is suitable for concrete design and production.

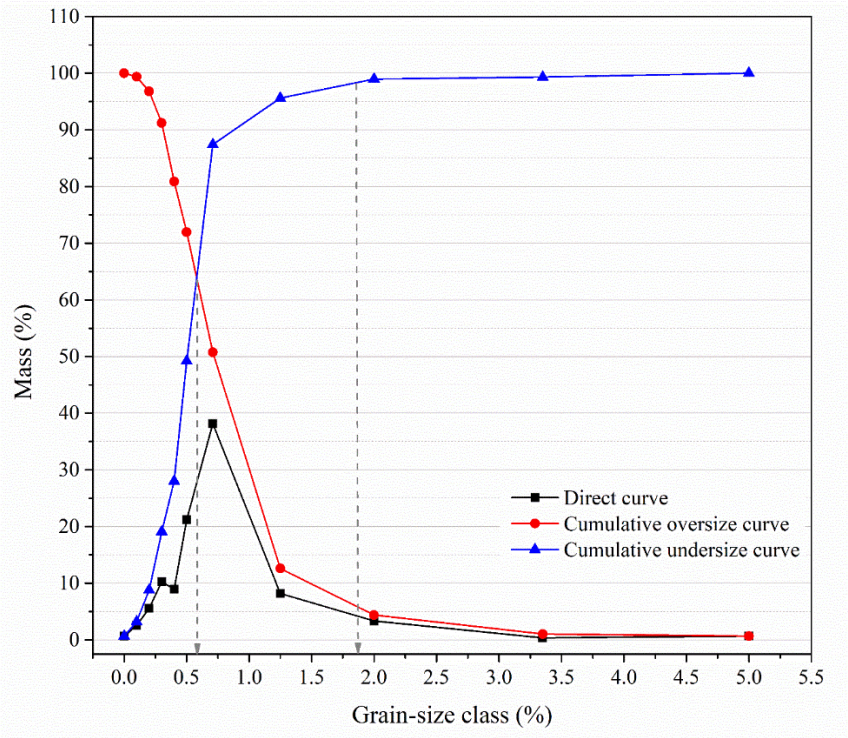

Figure 4. Grain-size distribution of the original Pb-Zn slag from Topilinca, Veles.

Preprints (www.preprints.org) | NOT PEER-REVIEWED | Posted: 28 November 2023 doi:10.20944/preprints202311.1730.v1

Chemical analysis was conducted in order to determine whether the initial Pb-Zn slag sample from Topilnica contains useful metals such as Pb and Zn, as well as precious metals such as Ag. Furthermore, the chemical composition of the sample should indicate whether the Pb-Zn slag samples can be prepared through a magnetic or gravimetric separation process to remove the present impurities. Also, the quantification of major oxides should indicate whether this waste material can be utilized as an alternative resource for the production of cement clinker, filler for mortar and concrete, or aggregate for concrete. Table 2 shows the results from chemical composition identification using the methods described in Chapter 2.4.

Table 2. Chemical analysis of Pb-Zn slag from Topilnica, Veles.

Oxide	SiO_2	Al_2O_3	CaO	MgO	Na_2O	K_2O	Fe_2O_3	TiO_2	LoI
Content (%)	17.43	7.43	12.39	2.135	0.391	0.565	47.68	0.503	5.98
Element	Pb (%)		Zn (%)		S (%)		Ag (ppm)		
Content	2.24		7.10		2.10		27.53		

The chemical analysis highlighted the relatively high content of lead (2.24%) and zinc (7.10%). The content of silver was approximately 27 ppm. Application of various separation and beneficiation methods for slag enrichment could increase the content of Pb, Zn, and Ag, which would lead to their further exploitation. The chemical composition analysis indicates that micronized slag could be used as an addition in cement clinker production [38–42] or, alternatively, as a non-reactive filler or coarse aggregate in concrete [43–50]. The presence of sulfur in the Pb-Zn slag sample in the amount of 2.10% in the form of sulfides or sulfates, which reacted with oxygen from the air at high temperatures (up to 1000 °C), resulted in the formation of new compounds and an increase in mass. This information may be useful in determining the best technological procedure for separating valuable elements in Pb-Zn slag from existing impurities. However, because the total sulfur content is less than 2.75%, this slag can be used as an addition to cement as well as aggregate in concrete mix design [51,52].

The X-ray diffraction analysis of the pulverized Pb-Zn sample is illustrated in Figure 5.

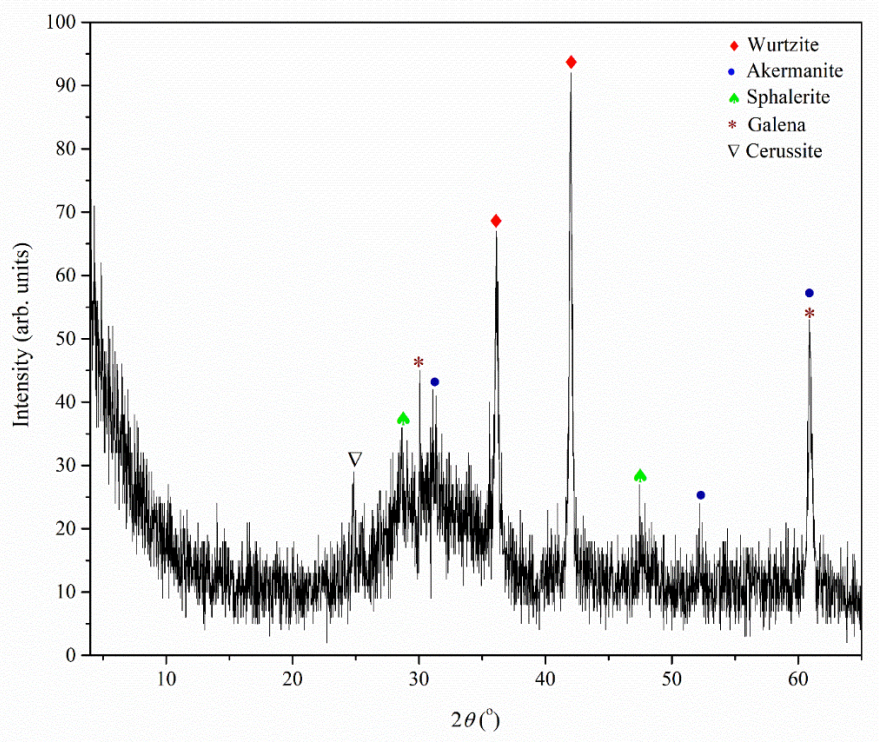

Figure 5. XRD diffractogram of Pb-Zn slag.

 doi:10.20944/preprints202311.1730.v1

The presence of the following phases was determined in the analyzed sample: amorphous phase, wurtzite, sphalerite, galena, cerussite, and akermanite. The most abundant phase in the analyzed sample is the amorphous phase, while wurtzite and all other phases are significantly less represented. The amorphous phase can be related to alumosilicates created as byproducts of ore melting. Wurtzite is a structural polymorph form of sphalerite that is less commonly encountered. It is a zinc and iron sulfide mineral with the chemical formula (Zn,Fe)S. There is variation in the iron content up to 8%. Along with matraite and sphalerite, it is trimorphous. Wurtzite is typically found as massive, resinous, dark reddish-brown, black to dark reddish-brown, botryoidal banded crusts, and, less frequently, as hemimorphic pyramidal, or tabular, crystals. There are several known polytypes, the most prevalent of which is the hexagonal 2H polytype. The ones for 4H, 6H, 8H, 10H, and 15R are also mentioned by Haussühl and Müller (1963) [53–55]. Wurtzite hardness is 3½–4, which is less than quartz (7 on the Mohs scale of hardness), the main constituent of sand and gravel used for concrete. Zinc sulfide (ZnS) mineral sphalerite has a bronze-black and honey-yellow hue. In its pure state, the mineral has 67% zinc metal. It is the most significant zinc ore. The majority of the sizable zinc deposits of the SEDEX (Sedimentary Exhalative) type are linked to the mineralization of lead, copper, silver, cadmium, nickel, and gold. Sphalerite has relatively low hardness (3.5–4.0 Mohs scale) [52,54]. Galena ($Pb^{2+}S^{2-}$ or PbS) is a mineral that contains lead sulfide. It is the world's most important lead ore and a significant silver ore. It can be found in skarns, sedimentary rocks, pyrite, chalcopyrite, sphalerite, tennantite-tetrahedrite, and other ore veins. It can also be deposited in pore spaces or replace carbonate beds in sedimentary rocks. When fresh, the crystals are bright, but exposure to air frequently causes them to tarnish. Galena has a Mohs hardness range of 2.50 to 2.75, making it moderately soft [54,56]. Cerussite ($PbCO_3$) is a mineral composed of lead carbonate that is typically found in the oxidized zone of lead ore deposits. It has a Mohs hardness of 3 to 3.75. It is a common aging product of galena and other lead ore minerals weathering. The mineral cerussite is interesting because it can form in a variety of intriguing crystal formations with odd twinning habits. Its massive weight, brilliant luster, and crystal habits make it easy to identify. Because they could be delicate, specimens need to be handled carefully [54,56,57]. Akermanite, a mineral composed of dicalcium magnesium disilicate, $Ca_2MgSi_2O_7$, is a member of the melilite mineral series. Melilite is a group of sorosilicate minerals made up of calcium silicates of magnesium and aluminum; the magnesian end-member is åkermanite, and the aluminous end-member is gehlenite. These minerals crystallize from a variety of artificial melts, blast-furnace slags, and calcium-rich alkaline magmas. The most common places to find them are in contact zones of thermally metamorphosed limestones and in impure carbonate rocks that have been transformed into feldspathoidal rocks by basic magmas. Åkermanite is classified as a 5 or 6 on the Mohs mineral hardness scale [58,59]. According to the mineral hardness, which is comparatively lower than that of standard aggregate for concrete, during crushing and subsequent milling, mineral materials mostly end up in the fine aggregate share (i.e., sand or filler), while crushed glassy content will form the coarse aggregate share.

Several samples of Pb-Zn slag were observed using optical microscopy on Carl Zeiss-Jena's JENAPOL-U polarizing microscope. The samples were distributed on a plexiglass carrier and observed in transmitted or reflected light. The microphotographs of the samples are provided in Figure 6. The details visible in the microphotographs of the slag samples are as follows: a) Spherical lead alloy inclusions in a glassy matrix (recorded in air and reflected light); b) Complex fusion of Pb-Zn alloys with sphalerite, galena, and dark gray inclusions of cerussite (recorded in air and reflected light); c) Complex fusion of Pb-Zn alloys with sphalerite, galena, and wurtzite (recorded in air and reflected light); d) A simple fusion of a lead alloy with a vitreous matrix (recorded in air and reflected light); e) A simple fusion of sphalerite and amorphous matter (recorded in air and reflected light); f) Inclusions of elemental silver (shiny white dots) in the glassy matrix (recorded in oil and reflected light); g) An inclusion of elemental copper in the glassy matrix (recorded in oil and reflected light); h) Inclusions of elemental silver (shiny white dots) in the glassy matrix (recorded in oil and reflected light); i) An inclusion of elemental silver (shiny white dot) in the glassy matrix (recorded in oil and reflected light); j) Inclusions of elemental copper (bright reddish-yellow dots) in a glassy matrix (recorded in oil and reflected light); k) Oval inclusions of elemental silver (shiny white dots) in lead

 doi:10.20944/preprints202311.1730.v1

alloy (recorded in oil and reflected light); l) Inclusions of elemental silver (brilliant white) in lead alloy (recorded in oil and reflected light); m) An inclusion of elemental copper (bright orange) in a glassy matrix (recorded in oil and reflected light); n) Simple fusion of Pb-Zn alloys (recorded in air and reflected light).

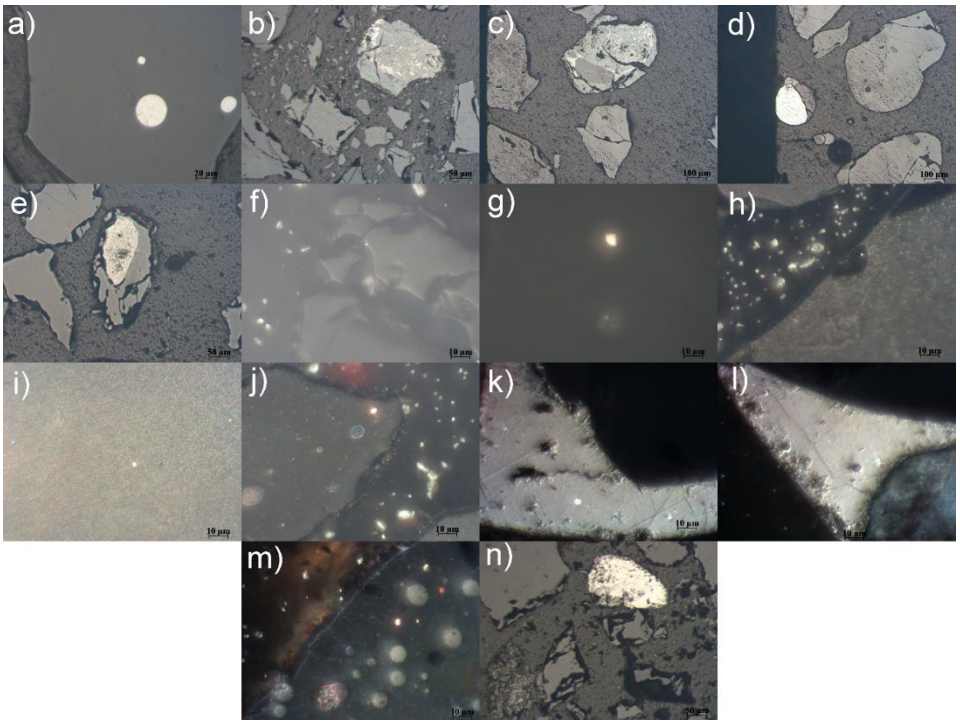

Figure 6. Microphotographs of Pb-Zn slag samples.

Based on the obtained qualitative mineralogical analysis, the following phase composition was determined: amorphous phase, lead alloys, zinc alloys, wurtzite, sphalerite, galena, cerussite, elemental silver, elemental copper, elemental iron, magnetite, spinel, rutile, hematite, troilite. The most common phase is the amorphous phase (glassy matrix) of spinel, silicate and mixed (spinel-silicate) composition, while wurtzite, which appears as skeletal formations in the glassy matrix, is significantly less abundant. Residues of zinc alloys and lead alloys can go back into refinement process which includes gravity concentration and magnetic separation procedures, in order to separate unable Zn and Pb. This is a step towards closing a recycling circle. Similar procedures can be applied to elemental silver and copper. The rest of the materials can be employed as aggregate or filler in concrete manufacturing.

An even more precise preview of the microstructure of Pb-Zn slag is given in SEM microphotographs (Figure 7). The EDS analysis of the characteristic points and areas is also provided in the SEM images (Figure 7). The elemental analysis is provided in Table 3.

Preprints (www.preprints.org) | NOT PEER-REVIEWED | Posted: 28 November 2023 doi:10.20944/preprints202311.1730.v1

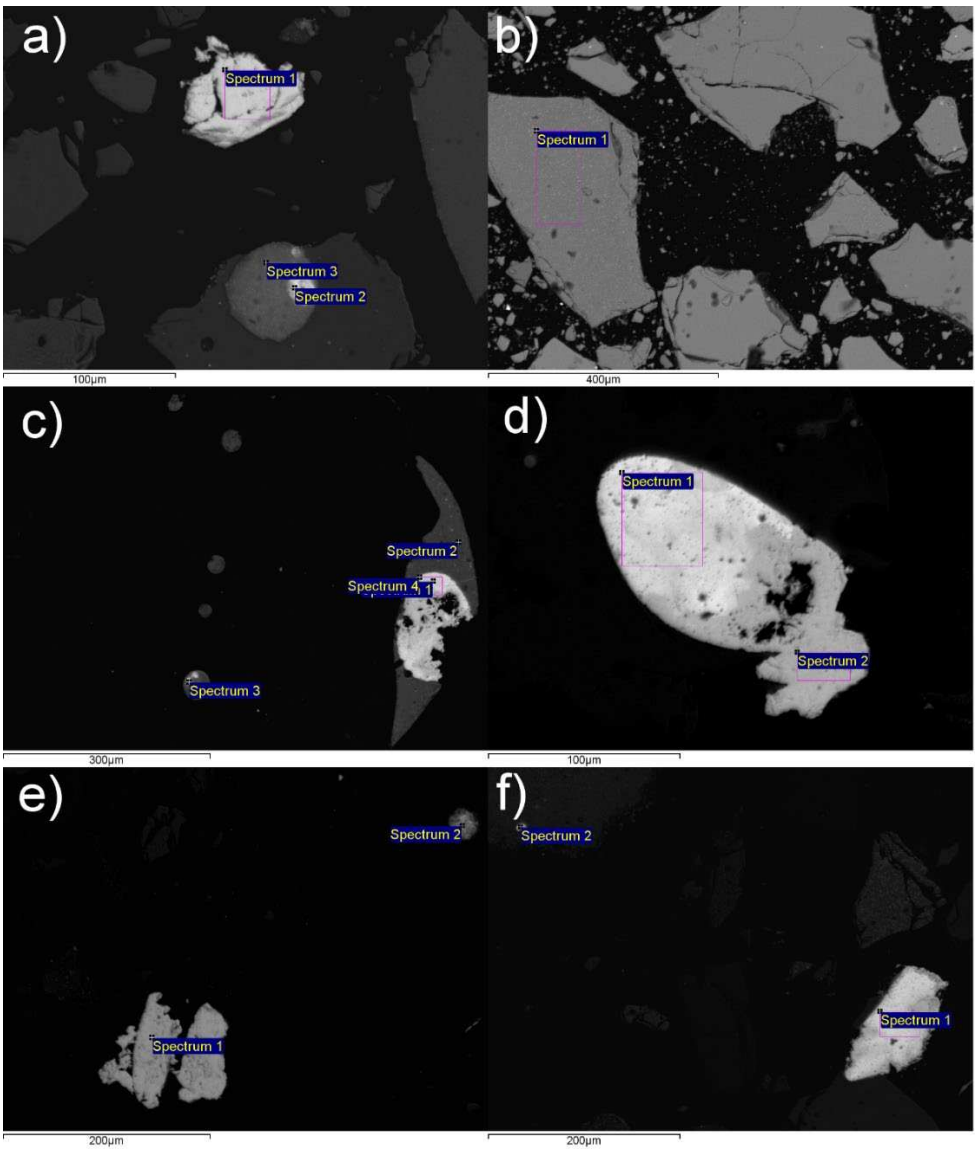

Figure 7. SEM microphotograph of PB-ZN slag sample: a) oxidized lead alloys; b) vitreous matrix; c) oxidized lead alloys; d) oxidized lead alloys; e) oxidized copper-zinc alloy; f) oxidized lead alloys.

SEM analysis combined with EDS elemental mapping revealed that the Pb-Zn slag sample is primarily composed of Fe-Mn-Zn spinel variants. Lead and zinc alloys are the next most abundant mineral phase categories. These alloys are predominantly combined by relatively small quantities of copper (0.37-3.5%, except in samples 7a/2, 7e/1, and 7e/2 where Cu content is elevated and it sums up to: 16.77%, 36.97%, and 32.21%, respectively). Lead and zinc alloy phase grains can be up to 100 µm in diameter. They are most commonly recognized as single particles or simple to complex inclusions in a glassy matrix composed of elemental iron and wurtzite. Grains larger than µ100 m in diameter are mostly free or in the form of simple inclusions. The largest diameters of these phases go up to 300 µm. Lead alloys almost always take the shape of regular spheres (Figures 7a and 7d). Small quantities of visible and "invisible" (structural) silver were determined in oxidized copper-zinc alloy (Figure 7e) and oxidized lead alloy (Figure 7f). According to these analyses, only a small percentage of lead alloys and copper-zinc alloys (about 10%) contain elemental silver with a content of up to 1%. Silver particles are usually oval-shaped, but it can also be found in the form of tiny wires with lengths of up to 5 µm. Aside from the alloys, elemental silver and copper occur as small inclusions in the glassy matrix and wurtzite, rarely exceeding 2-3 µm (silver) and 7-8 µm (copper). It is important to note that elemental silver is frequently found in host grain cracks. Galena and sphalerite are in a subordinate position in relation to Pb and Zn alloys, and they are almost exclusively found in the form of simple

Preprints (www.preprints.org) | NOT PEER-REVIEWED | Posted: 28 November 2023 doi:10.20944/preprints202311.1730.v1

to complex inclusions with these alloys. Cerussite has been identified in traces and is only found in simple to complex aggregates or even inclusions with sphalerite. Iron, in addition to wurtzite, magnetite, hematite, troilite, and spinel, occurs in elemental form, but also in trace amounts as pyrite and arsenopyrite.

Table 3. Chemical analyzes of selected grains of the Pb-Zn slag sample (EDS method).

Point in Figure7	Pb (%)	Cu (%)	Fe (%)	As (%)	Sb (%)	O (%)	Fe (%)	Ca (%)	Si (%)	Al (%)	Zn (%)	Ag (%)
7a/1	75.23	0.79	0.70	-	-	22.40	-	-	-	-	-	-
7a/2	55.73	16.77	3.76	1.1	13.30	8.62	-	-	-	-	-	-
7a/3	68.41	0.92	0.60	-	-	31.54	-	-	-	-	-	-
7b/1	-	0.60	-	-	-	30.30	29.05	7.03	18.26	12.45	16.67	-
7c/1	82.69	2.36	-	-	-	14.95	-	-	-	-	-	-
7c/2	80.25	1.98	-	-	-	15.98	-	-	-	-	-	-
7c/3	78.74	2.56	-	-	-	16.78	-	-	-	-	--	
7c/4	79.05	3.50	0.95	-	-	16.50	-	-	-		-	-
7d/1	84.62	2.36	-	-	-	13.01	-		-		-	-
7d/2	76.23	-	0.54		-	21.81	-	1.41	-	-	-	-
7e/1	-	36.97	8.94	-	-	8.81	-	2.53	3.56	1.28	33.10	0.91
7e/2	-	32.21	6.57	-	-	9.25	-	1.57	2.89	1.54	38.41	0.74
7f/1	90.70	0.46	-	-	-	7.76	-	-	-	-	-	0.97
7f/2	91.4	0.37	-	-	-	8.54	-	-	-	-	-	0.82

A plan for the next stage of the experiment is to try to condense the nonferrous metals into a collective concentrate from which the biggest quantity of silver might be extracted. These tests should be carried out using gravity concentration and magnetic separation techniques. Most elemental iron, magnetite, and wurtzite, as well as amorphous phases of spinel and ferrite compositions that contain iron in their structure, should be removed by magnetic separation. Gravitational concentration should separate nonferrous metal concentrates from the nonmagnetic glassy matrix.

3.1. Application of Pb-Zn slag in construction materials

In order to transition to a more circular economy, it is imperative that waste materials from metallurgy be reused more often. This has resulted in numerous examples of these materials being used as additives or aggregates in building materials, including cement, mortars, concrete, masonry bricks, and geopolymers [20–26]. The analyzed Pb-Zn slag's high concentration of alumo-silicate amorphous phase and strength-giving iron-based minerals are good signs that the material could be used for producing building materials. An experimental material must meet specific requirements for standard building materials before it can be used in the construction industry (e.g., EN standards or their national versions are often applied). Therefore, initial testing is carried out on the production of cement mortars that include Pb-Zn slag.

For the experiment, four cement mortar samples were prepared. The bonding agent employed in all mortar samples was ordinary Portland cement (OPC) (CEM I 42.5R, Lafarge - specific surface area 292 m^2/kg; 97.5 % of particles less than or equal to 0.63 mm). The CEM - N mortar sample was used for comparison of the results. High-purity silica sand (SiO_2 = 98.1%; Mohs hardness 7; uncompacted bulk density 1640 kg/m^3 and compacted bulk density 1750 kg/m^3) was utilized as aggregate in the CM-N sample. Pulverized Pb-Zn slag was used as a mineral addition in the CEM-PbZn10, CEM-PbZn20, and CEM-PbZn30 samples. This raw material is employed both as filler (due to its small average grain diameter, i.e., d50 = 10μm) and possibly as a replacement for the binder

 doi:10.20944/preprints202311.1730.v1

(due to its vitreous Al-Si origin). As aggregate, crushed Pb-Zn slag (grain sizes 0.063–4.0 mm) was used. The grain size distribution was: 0.063 - 0.5 mm = 30%, 0.5–1.0 mm = 40%, 1.0–2.0 mm = 20%, and 2.0–4.0 mm = 10%. Mohs hardness of Pb-Zn slag was approximately 6 due to the high Fe_2O_3 content (Table 2) and presence of iron-based-minerals (Figure 5), which makes it a good substitution for quartz sand. The chemical composition of the cement was determined using the XRF technique (the method was described in Chapter 2.4): SiO_2 = 21.95%; Al_2O_3 = 5.41%; Fe_2O_3 = 3.05%; CaO = 61.98%; MgO = 2.69%; K_2O = 0.91%; Na_2O = 0.10%; TiO_2 < 0.1%; SO_3 = 2.15%; loss on ignition at 1000 °C = 0.96%. The mix design of the experimental mortars is provided in Table 4.

Table 4. Mix-design of the experimental mortar samples.

Sample	OPC (%)	Pb-ZN slag - coarse fraction (%)	Pb-ZN slag - Pulverized (%)	Natural aggregate - quartz sand (%)
CEM-N	40	-	-	60
CEM-PbZn10	36	60	4	-
CEM-PbZn20	32	60	8	-
CEM-PbZn30	28	60	12	-

Mortar samples were prepared using the standard procedure [60] according to the mix design shown in Table 4. Using a laboratory mixer, cement, aggregate, and filler were initially dry-homogenized. Water was added later in the mixing process. Fresh mortar was placed in steel molds (40×40×160 mm) and stored for one day in a climate chamber (95±5% relative humidity and 20°C (+3°C/-2°C) temperature. Upon removal from the molds, samples were stored in the climate chamber under the same conditions for a total of 7 days. Following that, the samples were cured for 21 days at 65±5% relative humidity. The rheology of the fresh mortar was determined via a slump test using a flow table [61]. Bulk density of fresh mortar and dry bulk density of hardened mortar [62,63], determination of water absorption coefficient due to capillary action of hardened mortar [64], and compressive and flexural strengths [65] were determined using standard methods. All obtained testing results represent an average of at least three tests.

Experimentally determined physico-mechanical properties of fresh and hardened mortar samples (workability of fresh mortar in mm; bulk density of fresh mortar in kg/m^3; bulk density of hardened mortar in kg/m^3; and water absorption coefficient in mg/m^2·min$^{0.5}$) are illustrated in graphs provided in Figure 8.

In comparison to standard cement mortar, the workability of fresh mortar samples increased with the addition of Pb-Zn slag filler (the workability of the CEM-N sample was 187 mm). CEM-PbZn20 has the highest workability value (195 mm), indicating that adding more than 20% filler has a negative impact on the physico-mechanical properties of mortars in their fresh state. Bulk density, measured both in fresh and hardened states, showed an increasing trend. CEM-PbZn10, CEM-PbZn20, and CEM-PbZn30 samples had higher bulk density values than CEM-N (2200 kg/m^3 and 2140 kg/m^3 – in fresh and hardened state, respectively). Because of the difference in specific gravities of aggregates, the bulk densities in the fresh state of mortars with slag are 150, 180, and 190 kg/m^3 higher for the CEM-PbZn10, CEM-PbZn20, and CEM-PbZn30 samples, respectively. Namely, the specific gravity of Pb-Zn slag varies between 2500 and 3600 kg/m^3 [66], while the specific gravity of silica sand is usually 1730–1750 kg/m^3 [67]. The differences between bulk densities in the hardened state were similar: 130, 140, and 150 kg/m^3 for the CEM-PbZn10, CEM-PbZn20, and CEM-PbZn30 samples, respectively. The addition of fine Pb-Zn slag, as well as the substitution of standard aggregate with coarse Pb-Zn slag aggregate, influenced the increase in bulk densities. Pb-Zn mortar samples had lower water absorption coefficients than standard mortar (CEM-N). The values of the water absorption coefficient are decreasing with increasing content of Pb-Zn filler. The addition of filler aided in better 'packing' of the microstructure, leaving fewer voids and pores behind, lowering the examined material's water absorption capability [68,69].

Preprints (www.preprints.org) | NOT PEER-REVIEWED | Posted: 28 November 2023 doi:10.20944/preprints202311.1730.v1

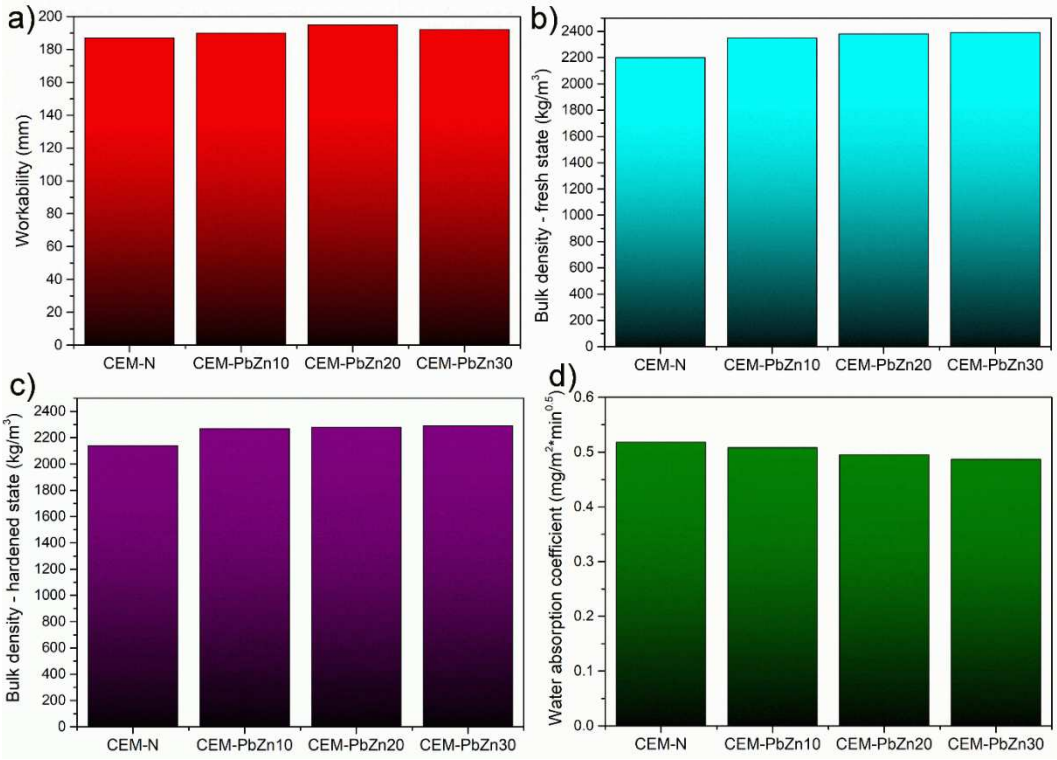

Figure 8. Physico-mechanical properties of mortar samples: a) workability, b) bulk density of fresh mortar, c) bulk density of hardened mortar, d) water absorption coefficient.

Values of mechanical strengths (CS – compressive strength and FS – flexural strength) measured after 2, 7, and 28 days of hardening are provided in Figure 9.

As shown in Figure 9, differences in initial compressive strengths were more pronounced during the early stages of mortar hardening. After two days of hardening, the compressive strength of the CEM-PbZn10 sample was 25% higher than the CS-2 of the standard mortar sample (CEM-N). There was a 35.6% difference in CS-2 between CEM-PbZn20 and CEM-N, and a 30% difference between CEM-PbZn30 and CEM-N. For CEM-PbZn10, CEM-PbZn20, CEMPnZn30, and CEM-N, the differences in the final 28-day strengths (CS-28) were 14.14%, 23.8%, and 17.9%, respectively. A higher increase in initial strengths can be explained by the pozzolanic effect of PB-Zn slag filler [70]. The CEM-PbZn20 sample has the highest final compressive strength (CS-28 = 53.05 MPa), indicating that the Pb-Zn filler contributes the most in its quantity of 20%. Thereby, over 20% of slag-based filler content has no beneficial effect on mechanical strengths.

Flexural strengths showed a similar distribution of strengths in the diagram (Figure 9). Namely, the CEM-PbZn20 sample yielded the highest values for FS-2 and FS-28 (3.5 and 8 MPa, respectively). The difference in initial flexural strengths of slag-based mortars and cement mortars was 2%, 10%, and 8% for CEM-PbZn10, CEM-PbZn20, and CEM-PnZn30, respectively. The final flexural strengths (FS-28) differed from CEM-N by 11%, 16%, and 15%, respectively.

Preprints (www.preprints.org) | NOT PEER-REVIEWED | Posted: 28 November 2023 doi:10.20944/preprints202311.1730.v1

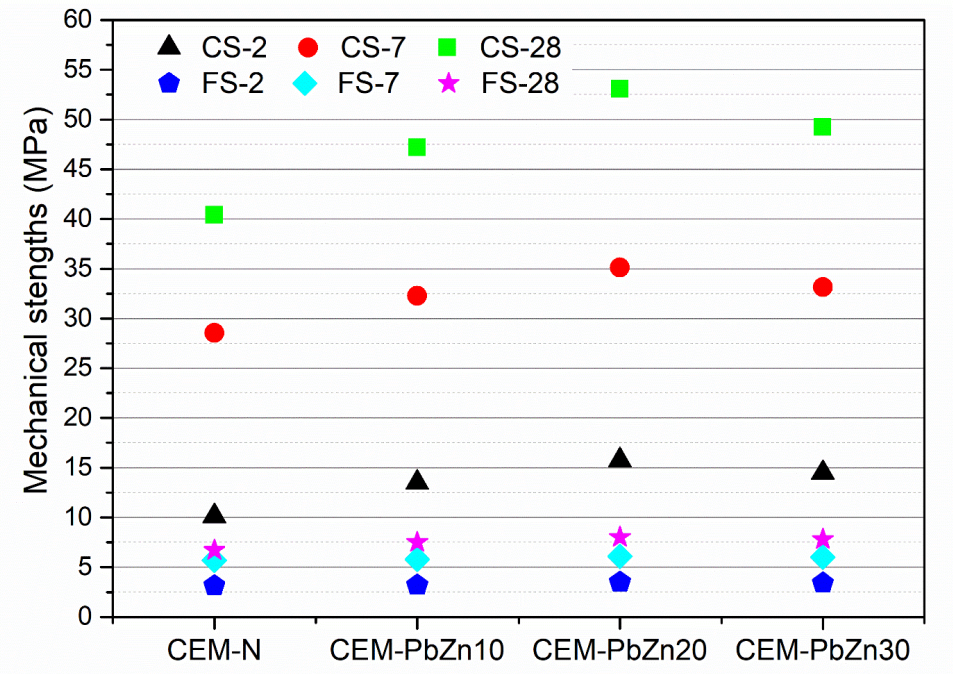

Figure 8. Mechanical strengths of mortar samples. (CS - compressive strength; FS - flexural strength, 2/7/28– days).

Pulverized Pb-Zn slag used as a filler contributed to the mechanical strengths of the tested mortars to a certain extent (i.e., 20% addition). The mechanical strengths of slag-based mortars CEM-PbZn10, CEM-PbZn20, and CEM-PnZn30 were also enhanced by the high hardness and bulk density of coarse aggregate made of Pb-Zn slag.

4. Discussion

Authors should discuss the results and how they can be interpreted from the perspective of previous studies and of the working hypotheses. The findings and their implications should be discussed in the broadest context possible. Future research directions may also be highlighted.

5. Conclusions

This The historic Pb-Zn slag from the smelter plant (Topilnica, Veles) was characterized based on physicochemical and mineralogical properties, and potential applications are proposed. The obtained results will serve as the foundation for more extensive technological tests that will define the procedure for refining Pb-Zn slag, separating non-ferrous metals and silver, and obtaining commercial building products, with the ultimate goal of closing the slag's life cycle in accordance with net-zero and zero-waste principles. The main conclusions are summarized below:

1) The cost-effectiveness of further refinement and the possibility of extracting valuable metals are considered due to the relatively high content of lead (2.24%), zinc (7.10%), and silver (27 ppm) in this waste material.
2) In the Pb-Zn slag sample, mineralogical analysis revealed an amorphous phase, lead alloys, zinc alloys, wurtzite, sphalerite, galena, cerussite, elemental silver, elemental copper, elemental iron, magnetite, spinel, rutile, hematite, and troilite. The amorphous phase (glassy matrix) of spinel, silicate, and mixed (spinel-silicate) composition is the most common, followed by wurtzite in the form of skeletal formations in the glassy matrix. Pb and Zn can be recovered from zinc and lead alloys residues via the refinement process, which includes gravity concentration and magnetic separation procedures, thus closing the recycling circle. Elements like silver and copper can be treated in the same way.
3) The high concentration of alumo-silicate amorphous phase and strength-giving iron-based minerals in the analyzed Pb-Zn slag indicate that the material could be used for the production of building

materials. Namely, the amorphous spinel, silicate, and mixed spinel-silicate phases of slag, which contain high concentrations of SiO_2, Al_2O_3, CaO, and Fe_2O_3, are suitable for producing cement clinker, mineral fillers, or coarse aggregate for concrete or mortar.

4) The study revealed that producing Pb-Zn slag-based mortar with 20% of pulverized slag as a maximum cement replacement and 60% slag aggregate in the mix-design is feasible. Namely, CEM-PbZn10, CEM-PbZn20, and CEMPnZn30 mortars had final 28-day strengths that were 14.14%, 23.8%, and 17.9% higher than standard cement mortar. The high hardness and bulk density of coarse aggregate made of Pb-Zn slag increased the mechanical strengths of the slag-based mortars CEM-PbZn10, CEM-PbZn20, and CEM-PnZn30. The final compressive strength of the CEM-PbZn20 sample is the highest (CS-28 = 53.05 MPa), indicating that the Pb-Zn filler contributes the most in its quantity of 20%.
5) The study demonstrated that metallurgy waste can be refined and reused. In terms of circular economy principles, Pb-Zn slag has a high re-utilization potential, so it is critical to thoroughly investigate the material and establish methods and preparation processes, as well as methods of concentrating useful components into commercial products.

Author Contributions: Conceptualization, D.R. and A.T.; methodology, D.R., A.T., and J.S.; validation, D.R., A.T., and J.S.; formal analysis, D.R., J.S., V.J., D.T. and B.I.; investigation, D.R., A.T. and J.S.; writing—original draft preparation, A.T. and D.R.; supervision, A.T. All authors have read and agreed to the published version of the manuscript.

Funding: This research was funded by the Ministry of Science, Technological Development and Innovation of the Republic of Serbia (Contract No.: 451-03-47/2023-01/200012) and Project: 101111694 — GREENCO — ERASMUS-EDU-2022-PI-ALL-INNO.

Institutional Review Board Statement: Not applicable.

Informed Consent Statement: Not applicable.
Data Availability Statement: Not applicable.
Acknowledgments: The authors gratefully appreciate support from the projects financially supported by the Ministry of Science, Technological Development and Innovation of the Republic of Serbia (Contract No.: 451-03-47/2023-01/ 200012) and 101111694 — GREENCO — ERASMUS-EDU-2022-PI-ALL-INNO).

Conflicts of Interest: The authors declare they have no competing interest or financial conflict among them.

References

1. Chen, D.T.; Roy, A.; Li, Y.; Bogush, A.; Au, W.Y.; Stegemann, J. Speciation of toxic pollutants in Pb/Zn smelter slags by X-ray Absorption Spectroscopy in the context of the literature. *J. Hazard. Mater*. 2023, 460, 132373. https://doi.org/10.1016/j.jhazmat.2023.132373
2. Web-site: www.statista.com
3. Kania, H.; Saternus, M. Evaluation and Current State of Primary and Secondary Zinc Production—A Review. *Appl. Sci.* 2023, 13, 2003. https://doi.org/10.3390/app13032003
4. Web site: https://www.teck.com/media/Carbon-Footprint-of-Teck-Special-High-Grade-Zinc.pdf
5. Bača, P.; Vanýsek, P. Issues Concerning Manufacture and Recycling of Lead. *Energies* 2023, 16, 4468. https://doi.org/10.3390/en16114468
6. EPA web-site: https://www.epa.gov
7. Buch, A.C.; Niemeyer, J.C.; Marques, E.D.; Silva-Filho, E.V. Ecological risk assessment of trace metals in soils affected by mine tailings. *J. Hazard Mater.* 2021, 403, 123852. https://doi.org/10.1016/j.jhazmat.2020.123852
8. Nowińska K.; Zdzisław A., Slags of the Imperial Smelting Process for Zn and Pb Production. In: Saleem Hashmi (editor-in-chief), In *Reference Module in Materials Science and Materials Engineering*. Oxford: Elsevier; 2017. pp. 1-5. ISBN: 978-0-12-803581-8 https://doi.org.10.1016/B978-0-12-803581-8.03607-9
9. Sun, Z.; Hu, Y.; Cheng, H. Public health risk of toxic metal(loid) pollution to the population living near an abandoned small-scale polymetallic mine. *Sci. Total Environ*. 2020. 718, 137434. https://doi.org/10.1016/j.scitotenv.2020.137434
10. Safa, M.; Goodarzi, A.; Lorestani, B. Enhanced post freeze-thaw stability of Zn/Pb co-contaminated soil through MgO-activated steel slag and fiber treatment, *Cold Regions Sci. Technol.* 2023, 210, 103826. https://doi.org/10.1016/j.coldregions.2023.103826,
11. Ettler, V.; Johan, Z. 12 years of leaching of contaminants from Pb smelter slags: Geochemical/mineralogical controls and slag recycling potential. *Applied Geochemistry* 2014, 40, 97–103 http://dx.doi.org/10.1016/j.apgeochem.2013.11.001

12. Wang, W., Gan, Y., Kang, X., Synthesis and characterization of sustainable ecofriendly unburned bricks from slate tailings. *J. Mater. Res. Technol*. 2021. 14, 1697–1708. https://doi.org/10.1016/j.jmrt.2021.07.071
13. Wang, P.; Li, J.; Hu, Y.; Cheng, H. Solidification and stabilization of Pb–Zn mine tailing with municipal solid waste incineration fly ash and ground granulated blast-furnace slag for unfired brick fabrication, *Environ. Pollut.* 2023, 321, 121135, https://doi.org/10.1016/j.envpol.2023.121135.
14. Han, L.-J., Li, J.-S., Xue, Q., Guo, M.-Z., Wang, P., Poon, C.S., Enzymatically induced phosphate precipitation (EIPP) for stabilization/solidification (S/S) treatment of heavy metal tailings. Construct. Build. Mater. 2022, 314, 125577. https://doi.org/10.1016/j.conbuildmat.2021.125577
15. Fawzy, M.; El Ghar, S.; Gaafar, I.; El shafey, A.; Diab, M.; Hussein, A. Recovery of valuable heavy minerals via gravity and magnetic separation operations from Diit Quaternary stream sediments, southern coast of the Red Sea, Egypt, In Journal of Physics: Conference Series 2305. 2022, 012020 doi:10.1088/1742-6596/2305/1/012020
16. Huston, D. L.; Stevens, B.; Southgate, P.N; Muhling, P.; Wyborn, L. Australian Zn-Pb-Ag Ore-Forming Systems: A Review and Analysis, *Economic Geology* 2006, 101(6), 1117-1157, DOI: 10.2113/gsecongeo.101.6.1117
17. Alzhanova, G.Z.; Aibuldinov, Y.K.; Iskakova, Z.B.; Khabidolda, S.M.; Abdiyussupov, G.G.; Omirzak, M.T.; Murali, G.; Vatin, N.I. Development of Environmentally Clean Construction Materials Using Industrial Waste. *Materials* 2022, 15, 5726. https://doi.org/10.3390/ma15165726
18. Monteiro, N.B.R., da Silva, E.A., Moita Neto, J.M., Sustainable development goals in mining. J. *Clean. Prod.* 2019, 228, 509–520. https://doi.org/10.1016/j.jclepro.2019.04.332
19. Web-site: https://unfoundation.org/what-we-do/issues/sustainable-development-goals/
20. Kanneboina, Y.; Saravanan, J.; Kabeer, T.; Bisht, K. Valorization of lead and zinc slags for the production of construction materials - A review for future research direction. *Constr. Build. Mater.* 2023, 367, 130314. https://doi.org/10.1016/j.conbuildmat.2023.130314
21. Anandaraj, S.; Karthik, S.; Vijaymohan, S.; Rampradheep, G.; Indhiradevi, P.; Anusha, G. Effects of using white flour, zinc oxide and zinc ash as an admixture in mortar and concrete, *Mater. Today: Proceed.* 2022, 52, 1788-1793. https://doi.org/10.1016/j.matpr.2021.11.447.
22. Xu, L.; Sun, Z.; Tang, C.; Yang, K.; Li, B.; Zhang, Y.; Yang, Z.; Wu, K. Mitigation effect of accelerators on the lead–zinc tailing induced retardation in autoclaved concrete, *Constr. Build. Mater*. 2022. 352, 128929. https://doi.org/10.1016/j.conbuildmat.2022.128929.
23. Wang, H., Ju, C.; Zhou, M.; Zheng, F.; Dong, Y.; Hou, H.; Liu, S. Grinding kinetics of lead–zinc tailing powders and its optimal particle size as a pozzolanic admixture in cement mortar, *Adv. Powder Technol*. 2022, 33: 9, 103730. https://doi.org/10.1016/j.apt.2022.103730.
24. Murmu, A.L., Patel, A., Towards sustainable bricks production: an overview. *Construct. Build. Mater.* 2018. 165, 112–125. https://doi.org/10.1016/j.conbuildmat.2018.01.038
25. Chen, Y., Zhang, Y., Chen, T., Zhao, Y., Bao, S., Preparation of eco-friendly construction bricks from hematite tailings. *Construct. Build. Mater.* 2011. 25, 2107–2111. https://doi.org/10.1016/j.conbuildmat.2010.11.025
26. Zhao, Y., Zhang, Y., Chen, T., Chen, Y., Bao, S. Preparation of high strength autoclaved bricks from hematite tailings. *Construct. Build. Mater*. 2012. 28, 450–455. 10.1016/j.conbuildmat.2011.08.078
27. Wang, W., Gan, Y., Kang, X., Synthesis and characterization of sustainable ecofriendly unburned bricks from slate tailings. *J. Mater. Res. Technol.* 2021. 14, 1697–1708. https://doi.org/10.1016/j.jmrt.2021.07.071
28. Zhang, X.; Li, L.; Ul Hassan, Q.; Pan, D.; Zhu, G. Preparation and characterization of glass ceramics synthesized from lead slag and lead-zinc tailings. *Ceram. Intern.* 2023, 49, 16164–16173 https://doi.org/10.1016/j.ceramint.2023.01.214
29. Li, J.; Liu, Y.; Ke, X.; Jiao, X.; Li, R.; Shi, C. Geopolymer synthesized from electrolytic manganese residue and lead-zinc smelting slag: Compressive strength and heavy metal immobilization. *Cem. Concr. Comp.* 2022, 134, 104806. https://doi.org/10.1016/j.cemconcomp.2022.104806
30. Morrison, C.; Hooper, R.; Lardner, K. The use of ferro-silicate slag from ISF zinc production as a sand replacement in concrete, *Cem. Concr. Res*. 2003, 33, 2085-2089. 10.1016/S0008-8846(03)00234-5
31. Atzeni, C.; Massida, L.; Sanna, U. Use of Granulated Slag from Lead and Zinc Processing in Concrete Technology, *Cem. Concr. Res*. 1996. 26, 1381–1388. https://doi.org/10.1017/CBO9781107415324.004.
32. Buzatu, T.; Talpos, E.; Petrescu, M.; Ghica, V; Iacob, G; Buzatu, M. Utilization of granulated lead slag as a structural material in roads constructions, *J. Mater. Cycles Waste Manag*. 2015, 17, 707–717. https://doi.org/10.1007/s10163-014-0297-z.
33. Prasad, P.S.; Ramana, G.V. Imperial smelting furnace (zinc) slag as a structural fill in reinforced soil structures, *Geotext. Geomembranes*. 2016. 44. 406–428. https:// doi.org/10.1016/j.geotexmem.2016.01.009.
34. Mandin, D.; van der Sloot, H.A.; Gervais, C.; Barna, R.; Mehu, J. Valorization of leadzincprimary smelters slags, *Studies in Environmental Science* 1997. 71:7, 617-630. https://doi.org/10.1016/S0166-1116(97)80245-2.

35. Duan, X.; Li, X.; Li, Y.; Qi, X.; Li, G.; Lu, Z.; Yang N. Separation and stabilization of arsenic in copper smelting wastewater by zinc slag, *J. Clean. Prod.* 2021. 312. 127797. https://doi.org/10.1016/j.jclepro.2021.127797.
36. Saedi, A.; Jamshidi-Zanjani, A.; Darban, A.K.; Mohseni, M.; Nejati, H. Utilization of lead–zinc mine tailings as cement substitutes in concrete construction: Effect of sulfide content, *J. Build. Eng.* 2022 57 104865. https://doi.org/10.1016/j.jobe.2022.104865.
37. Chen, W.; Peng, R.; Straub, C.; Yuan, B. Promoting the performance of one-part alkali-activated slag using fine lead-zinc mine tailings, *Constr. Build. Mater.* 2020, 236, 117745, https://doi.org/10.1016/j.conbuildmat.2019.117745.
38. Doussang, L.; Samson, G.; Deby, F.; Huet, B.; Guillon, E.; Cyr, M. Durability parameters of three low-carbon concretes (low clinker, alkali-activated slag and supersulfated cement), *Constr. Build. Mater.* 2023, 407, 133511. https://doi.org/10.1016/j.conbuildmat.2023.133511.
39. Turkoglu, M.; Bayraktar, O.Y.; Benli, A.; Kaplan, G. Effect of cement clinker type, curing regime and activator dosage on the performance of one-part alkali-activated hybrid slag/clinker composites, *J. Build. Eng.* 2023, 68, 106164,https://doi.org/10.1016/j.jobe.2023.106164.
40. Gao, T. Dai, T.; Shen, L.; Jiang, L. Benefits of using steel slag in cement clinker production for environmental conservation and economic revenue generation, *J. Clean. Product.* 2021, 282, 124538. https://doi.org/10.1016/j.jclepro.2020.124538.
41. Cao, L.; Shen, W.; Huang, J.; Yang, Y.; Zhang, D.; Huang, X.; Lv, Z.; Ji, X. Process to utilize crushed steel slag in cement industry directly: Multi-phased clinker sintering technology, *J. Clean. Product.* 2019, 217, 520-529. ISSN 0959-6526,https://doi.org/10.1016/j.jclepro.2019.01.260.
42. Erdoğan, S.; Koçak, T. Influence of slag fineness on the strength and heat evolution of multiple-clinker blended cements, *Constr. Build. Mater.* 2017, 155, 800-810. https://doi.org/10.1016/j.conbuildmat.2017.08.120
43. Nemade, P.; Pasla, D.; Chandrappa, A. Durability assessment of concrete with natural and Linz Donawitz slag as coarse aggregates, *Constr. Build. Mater.* 2023, 400, 132617. https://doi.org/10.1016/j.conbuildmat.2023.132617.
44. Ramakrishna, J.; Gopi, R. Experimental investigation on partial replacement of cement and coarse aggregate by rice husk ash and steel slag in concrete, *Materials Today: Proceedings*, 2023, https://doi.org/10.1016/j.matpr.2023.08.340
45. Chen, Z.; Huang, L.; Yan, L.; Cai, H.; Luo, X.; Li, Y. Autoclaved steel slag coarse aggregate: A potential solution for sustainable concrete production, *Constr. Build. Mater.* 2023, 400, 2023, 132627, https://doi.org/10.1016/j.conbuildmat.2023.132627
46. Teymouri, E.; Wong, K. S.; Tan, Y.; Pauzi, N. Mechanical behaviour of adsorbent pervious concrete using iron slag and zeolite as coarse aggregates. *Constr. Build. Mater.* 2023, 388. https://doi.org/10.1016/j.conbuildmat.2023.131720.
47. Lai, M.H.; Chen, Z.H.; Wang, Y.H.; Ho, J.C.M. Effect of fillers on the mechanical properties and durability of steel slag concrete, *Constr. Build. Mater.* 2022, 335, 127495. https://doi.org/10.1016/j.conbuildmat.2022.127495
48. Ballari, S. O.; Raffikbasha, M.; Shirgire, A.; Thakur, L.S.; Thenmozhi, S.; Kumar, B. Replacement of coarse aggregates by industrial slag, *Materials Today: Proceedings*. 2023. https://doi.org/10.1016/j.matpr.2023.03.491.
49. Singh, P.; Roy, A. B. D.; Singh, H. Mechanical and durability properties of concrete incorporating weathered coarse Linz-Donawitz (LD) steel slag, *J. Build. Engin.* 2022, 61, 105301, https://doi.org/10.1016/j.jobe.2022.105301.
50. Sosa, I.; Thomas, C.; Polanco, I.A.; Setién, J; Sainz-Aja, J.A.; Tamayo, P. Durability of high-performance self-compacted concrete using electric arc furnace slag aggregate and cupola slag powder, *Cem. Concr. Compos.* 2022, 127, 104399, https://doi.org/10.1016/j.cemconcomp.2021.104399.
51. Zheng, S.; Lu, X.; Zhao, J.; He, R.; Chen, H.; Geng, Y. Influence of industrial by-product sulfur powder on properties of cement-based composites for sustainable infrastructures, *Constr. Build. Mater.* 2023, 367, 130171, https://doi.org/10.1016/j.conbuildmat.2022.130171.
52. Huang, S.; Pi, Z.; Cai, C.; Li, H. Utilization of high-sulfur iron ore tailings in cement mortar by considering the influence of curing temperature and tailing content, *J. Build. Engin.* 2023, 74, 106826, https://doi.org/10.1016/j.jobe.2023.106826.
53. Haussühl, S., Müller, G. (1963) Neue ZnS-Polytypen (9R, 12R und 21R) in mesozoischen Sedimenten NW-Deutschlands. Beiträge zur Mineralogie und Petrographie: 9: 28-39. [9R, 12R & 21R polytypes].
54. Web site: www.mindat.org
55. Galsin, J. S. Chapter 1 - Crystal Structure of Solids,Editor(s): Joginder Singh Galsin, In *Solid State Physics,* Academic Press, 2019, P 1-36, ISBN 9780128171035, https://doi.org/10.1016/B978-0-12-817103-5.00001-3.
56. Haldar, S.K. Chapter 1 - Minerals and rocks,Editor(s): S.K. Haldar, In *Introduction to Mineralogy and Petrology* (Second Edition), Elsevier, 2020, 1-51, ISBN 9780128205853, https://doi.org/10.1016/B978-0-12-820585-3.00001-6.

57. Sánchez-Navas, A.; López-Cruz, O.; Velilla, N.; Vidal, I. Crystal growth of lead carbonates: Influence of the medium and relationship between structure and habit, *J. Crystal Growth*, 2013, 376, 1-10, https://doi.org/10.1016/j.jcrysgro.2013.04.007.
58. Web site: www.britannica.com
59. Pracejus, B. IV/C - Oxides with Metal: Oxygen = 2 : 3 (M_2O_3 and related compounds),Editor(s): Bernhard Pracejus, In *The Ore Minerals Under the Microscope* (Second Edition), Elsevier, 2014, 738-789, ISBN 9780444627254, https://doi.org/10.1016/B978-0-444-62725-4.50015-6.
60. Standard: SRPS EN 1015-2:2008 Methods of test for mortar for masonry - Part 2: Bulk sampling of mortars and preparation of test mortars
61. Standard: SRPS EN 1015-3:2008 Methods of test for mortar for masonry - Part 3: Determination of consistence of fresh mortar (by flow table)
62. Standard: SRPS EN 1015-6:2008 Methods of test for mortar for masonry - Part 6: Determination of bulk density of fresh mortar.
63. Standard: SRPS EN 1015-10:2008/A1:2008 Methods of test for mortar for masonry - Part 10: Determination of dry bulk density of hardened mortar.
64. Standard: SRPS EN 1015-18:2008 Methods of test for mortar for masonry - Part 18: Determination of water absorption coefficient due to capillary action of hardened mortar.
65. Standard: SRPS EN 1015-11:2019 Methods of test for mortar for masonry - Part 11: Determination of flexural and compressive strength of hardened mortar.
66. Wang, G.C. 3 - Nonferrous metal extraction and nonferrous slags,Editor(s): George C. Wang, In The Utilization of Slag in Civil Infrastructure Construction, Woodhead Publishing, 2016, 35-61,ISBN 9780081009949, https://doi.org/10.1016/B978-0-08-100381-7.00003-3.
67. Malathy, R.; Rajagopal Sentilkumar, S.R.; Prakash, A.R.; Das, B.B.; Chung, I.-M.; Kim, S.-H.; Prabakaran, M. Use of Industrial Silica Sand as a Fine Aggregate in Concrete—An Explorative Study. *Buildings* 2022, *12*, 1273. https://doi.org/10.3390/buildings12081273
68. Terzić, A.; Radulović, D.; Pezo, M; Stojanović, J; Pezo, L.; Radojević, Z.; Andrić, Lj. Prediction model based on artificial neural network for pyrophyllite mechano-chemical activation as an integral step in production of cement binders, Constr. Build. Mater. 2020, 258, 119721. https://doi.org/10.1016/j.conbuildmat.2020.119721.
69. Hatungimana, D.; Taşköprü, C.; İçhedef, M.; Saç, M.M.; Yazıcı, S. Compressive strength, water absorption, water sorptivity and surface radon exhalation rate of silica fume and fly ash based mortar, J. Build. Engin. 2019, 23, 369-376. https://doi.org/10.1016/j.jobe.2019.01.011.
70. Wang, H.; Ju, C.; Zhou, M.; Chen, J.; Dong, Y.; Hou, H. Sustainable and efficient stabilization/solidification of Pb, Cr, and Cd in lead-zinc tailings by using highly reactive pozzolanic solid waste, *J. Environ. Manag*. 2022, 306, 114473, https://doi.org/10.1016/j.jenvman.2022.114473.